Periodic Chirality Transformations Propagating On Bacterial Flagella

Daniel Coombs,[1] Greg Huber,[2] John O. Kessler,[3] and Raymond E. Goldstein[3,4]

[1]*Theoretical Biology and Biophysics, Los Alamos National Laboratory, Los Alamos, New Mexico 87545*
[2]*Department of Physics, University of Massachusetts, Boston, Massachusetts 02125*
[3]*Department of Physics, University of Arizona, Tucson, Arizona 85721*
[4]*Program in Applied Mathematics, University of Arizona, Tucson, Arizona 85721*

(Received 13 February 2002; published 23 August 2002)

When a helical bacterial flagellum, clamped at one end, is placed in an external flow, it has been observed that regions of the flagellum transform to the opposite chirality, and travel as pulses down the length of the filament, the process repeating periodically [H. Hotani, J. Mol. Biol. **156**, 791 (1982)]. We propose a theory for this phenomenon based on a treatment of the flagellum as an elastic object with multiple stable configurations. The simplest possible implementation of the model accurately reproduces key features seen in experiment.

DOI: 10.1103/PhysRevLett.89.118102 PACS numbers: 87.16.Ac, 05.45.–a, 46.40.Cd, 87.16.Qp

During chemotaxis of certain bacteria (*E. Coli*, for example), the multiple, rotating helical flagella that provide thrust to the cells exhibit remarkable dynamics. They bundle and unbundle as their rotary motors episodically reverse rotational direction [1–3]. When its flagella are bundled a bacterium moves linearly, but the disintegration of the bundle upon motor reversal creates a tumbling event that effectively randomizes the cell's orientation. These alternating modes of ''run'' and ''tumble'' enable the cell to sample different chemical environments, and give rise to the familiar chemotactic trajectories [4].

A series of investigations [3] has shown that flagella take on helical shapes of differing pitch, radius, and handedness under differing mechanical and chemical conditions. In particular, it has been observed [2] that the motor reversal that initiates a tumbling event not only turns the flagella in the opposite manner, but also initiates a *chirality reversal*, eventually turning a left-handed helix that had been rotated counterclockwise into a right-handed helix rotated clockwise, as viewed from its distal end. In a set of elegant experiments, Hotani [5] studied detached *Salmonella* flagella that were irrotationally pinned to a microscope slide by one end, and found that a steady fluid flow of order microns per second (~ 1 wavelength/s) past a flagellum leads to a remarkable *periodic* chirality transformation along the filament (Fig. 1). The left-handed helix develops a growing right-handed domain at its upstream end. Once a significant fraction of the helix is in the new state, the upstream end reverts back to left-handed while the right-handed domain travels downstream, disappearing as it reaches the helix end. A new region of flipped chirality is nucleated roughly as the preceding one reaches the end. Remarkably, the process continues periodically, demonstrating the generation of oscillations from steady forcing within the low Reynolds number regime. Hotani observed that the left-handed (*normal*) state could alternate with either of two right-handed states (*semicoiled* or *curly 1*) depending on how the filament was attached to the glass. Important recent work by Turner *et al.* [6] using fluorescently labeled *E. coli* flagella has shown that *in vivo* the sequence of transformations is more complex than originally thought; for instance, the sequence normal → semicoiled → curly 1 → normal is typically seen on a single flagellum during one run-and-tumble cycle.

In explaining static polymorphism, Calladine [7] conceived of the flagellum as 11 protofilaments of polymerized flagellin, slightly twisted together similar to the strands of a rope. Assuming that each strand may exist in one of two states with different geometric properties, he found 12 possible helical configurations that minimize the elastic strain of the whole filament. Nine of these have been seen experimentally [8]. His argument relies on the bistability of flagellin itself, confirmed by recent crystallography [9–12]. No theory has yet been advanced to explain the *dynamics* of flagellar polymorphism.

Here we propose a theory for the dynamics of Hotani's observations, first in broad terms, developing ideas of Hotani and Purcell [13,14], and then in a fully quantitative way, modeling the flagellum as an elastic filament with the underlying multistability described above. Our study, part of a larger class of problems in the dynamics of

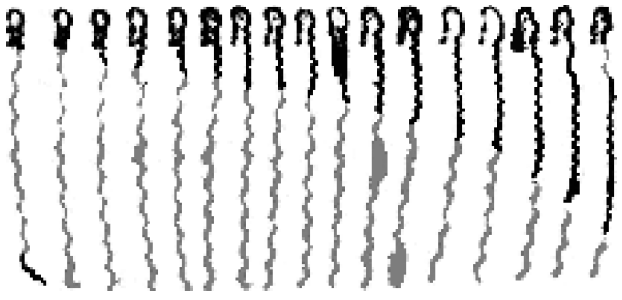

FIG. 1. Cyclic transformation between *normal* (grey) and *curly* (black) forms on a *salmonella* flagellum (length 23 μm). Time runs left-to-right at intervals of 0.55 s. Courtesy of Hotani.

biofilaments [15–17], raises the possibility that flagella conformations *in vivo* are associated in a self-consistent manner with the flows induced by swimming.

Consider a rigid helix of radius R, pitch P, filament radius a, and coiled length L held at $z = 0$ in a fluid of viscosity η with velocity field U along the z axis, which is the helix axis. The flow produces a tension and also a torque. In a local drag model [18], the torque density is σU, where $\sigma = (2\pi R^2 \zeta_\parallel)/(P^2 + 4\pi^2 R^2)^{1/2}$, $\zeta_\parallel \simeq \zeta_\perp/2 = 2\pi\eta/[\ln(L/2a) + c]$ are the drag coefficients for motions parallel and perpendicular to the filament, in the slender-body limit, and c is an order-one constant [19]. If the helix is static, the torque is maximum at the upstream end, decreasing to zero at the free end: $\tau(z) = \sigma U(L - z)$.

Suppose now we have two concatenated mirror-image helices. Purcell [13] observed that by cancellation of torques such a structure, sinking under its own weight in a viscous fluid, does not rotate. More generally, any set of concatenated helices in a flow has a piecewise linear torque profile and the rotary stress at its fixed end is specified entirely by the downstream configuration. In Hotani's experiment, that stress cycles in sign as pulses of oppositely handed helices move down the filament. One infers that it can alter the local monomer configuration and change the local handedness of the filament at the fixed end. Yet, these simple arguments do not explain the *dynamics* of polymorphism; for that, we must make reference to the *local* elastic strains [20].

Let the filament be aligned approximately with the z axis, with a shape $[X(z), Y(z), z]$ with $z \in (0, L)$. Imagine it is first straightened and untwisted and a stripe is painted along one side. In a twisted state, the stripe winds around the filament with an angle $\theta(z)$ $[\theta(0) = 0]$. We approximate the bend and twist rates Ω_i [20] as follows, using subscripts "z" to denote derivatives:

$$-i\Omega_1 + \Omega_2 = (X_{zz} + iY_{zz})e^{-i\theta}, \tag{1}$$

$$\Omega_3 \equiv \Omega = \theta_z. \tag{2}$$

The elastic energy E of a flagellum is modeled by $\int_0^L dz\, F(\Omega_1, \Omega_2, \Omega)$. The coarse-grained F incorporates filament multistability, and for a given flagellum has minima corresponding to locally stable states [7]. A simple functional describing multistable chirality is [21]

$$F = \frac{A}{2}[\Omega_1^2 + (\Omega_2 - Q)^2] + \frac{\gamma^2}{2}\Omega_z^2 + V(\Omega), \tag{3}$$

where A is the bend modulus, Q is the spontaneous curvature, and γ imposes a front width. Multistability appears through the minima of V. The monostable $V(\Omega) \sim k(\Omega - 2\pi/P)^2$ describes a filament whose ground state is a helix of pitch P. As a first step towards understanding *in vitro* [5] and *in vivo* [6] studies, especially periodically nucleated chirality fronts, we study a *bistable* model [21], where V is a symmetric double well with minima at $\pm 2\pi/P$. This describes mirror-image left- and right-handed helices, separated by a barrier of height H.

The two chief unknown parameters of the model are H and γ. Using the drag estimated as above, Hotani deduced the scale of torques acting on the pinned end of the flagellum. That same procedure allows us to estimate H as the work per unit length done by the torque acting through the angle that untwists the filament halfway; $H \sim \tau(2\pi/P)$, and $\tau = \sigma L U^*$, where U^* is the critical flow velocity to initiate a chirality flip, or

$$H \sim \frac{2\pi\sigma L U^*}{P}. \tag{4}$$

The methylcellulose solution used by Hotani has a viscosity 2 orders of magnitude greater than that of water, while the induced rotational frequencies of the flagella were less by that same factor than those generated by the cellular motors; the scale of torques *in vivo* and *in vitro* are comparable. Other experimental parameters [5] are $L \sim 15\ \mu$m, $P \sim 2\ \mu$m, $\zeta_\parallel \sim 1$ g/cm s, and $\sigma \sim 10^{-5}$ g/s. Expressing U^* as $\tilde{U}^*\ \mu$m/s, this yields $H \sim 4 \times 10^{-8}\tilde{U}^*$ erg/cm. With U^* a few microns per second, this result is in line with an earlier discussion [21].

Once nucleated, the chirality front invades the flagellum at some velocity v, changing the flagellum's energy at a rate $\tau\Delta\Omega v$, where $\Delta\Omega = 2(2\pi/P)$ is the difference in twist rates between the two stable states. The power dissipated scales as $\zeta_\perp L(\omega R)^2$, where ω is the angular speed of rotation of the filament downstream from the transition. Geometrically, $\omega = (2\pi/P)v$. Balancing these two powers at the critical flow rate U^*, we have

$$v \simeq \frac{P}{(P^2 + 4\pi^2 R^2)^{1/2}} U^*. \tag{5}$$

Thus, the propagation speed at the onset of transitions depends only on the geometry of the helix and the flow rate, and is strictly less than the background flow. Our result applies only to the invasion of the first polymorphic front into a filament of one handedness. Using values of $R = 1.0\ \mu$m and $P = 2.0\ \mu$m, which we use as our standard, we find that $v \sim 0.30U^*$. There is no experimental data for the behavior of the system near onset. Figure 2 shows that the onset of fronts in numerical experiments (described below) is in line with the scaling result (5).

Moving beyond scaling results, we construct dynamics of twist and bend by balancing elastic forces with translational drag and torques with rotational drag. Forces and torques are found by functional differentiation of E with respect to X, Y and θ. We make here the simplifying assumption that the fluid acts as a homogeneous drag in the z direction; elsewhere we discuss perturbation of the flow by the flagellum. Introducing $\xi(z) = X(z) + iY(z)$, the long-wavelength equations of motion are

$$\zeta_\perp(\xi_t + U\xi_z) = -A(\xi_{zz} - Qe^{i\theta})_{zz}, \tag{6}$$

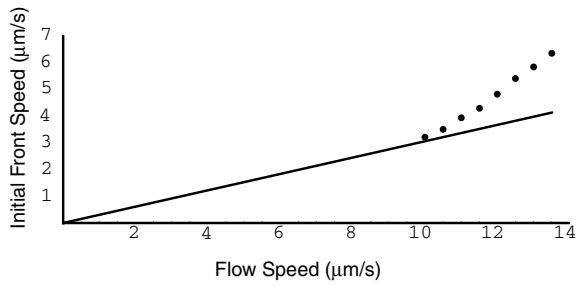

FIG. 2. Initial front velocity versus flow speed, comparing numerical results (dots) and Eq. (5) (solid line). The minimal flow speed for nucleation of fronts in the computations is 10 μm/s.

$$\zeta_r \theta_t = -\gamma^2 \theta_{zzzz} + V''(\theta_z)\theta_{zz} + A\,\mathrm{Im}(Qe^{i\theta}\xi^*_{zz}), \qquad (7)$$

where $\zeta_r = 4\pi\eta a^2$ is the rotational drag coefficient. Natural boundary conditions are a fixed, stress-free left end $\xi(0) = \theta(0) = \theta_{zz}(0) = 0$ and $\xi_{zz}(0) = Q$, with a completely free right-hand end: $\xi_{zz}(L) = e^{i\theta(L)}Q$, $\xi_{zzz}(L) = iQ\theta_z(L)e^{i\theta(L)}$, $\theta_{zz}(L) = 0$, $\gamma^2\theta_{zzz}(L) = V'[\theta_z(L)]$.

Without intrinsic bends or flow, (6) reduces to the simple elastic hyperdiffusion equation [22]. With intrinsic bends but without flow, the stationary solutions of (6) and (7) are of the form $\theta_0 = 2\pi z/P$, $\xi_0 = Q(P/2\pi)^2(1 - e^{iKz})$, where $V'(2\pi/P) = 0$; a helix of pitch P, chosen to pass through the origin. In the z direction, there are at least three length scales: $L \sim 15$ μm, $P \sim 2$ μm, and the front width we term λ, resulting from a balance of the twist-gradient energy with that of helix hand reversal: $\gamma^2\theta_{zzzz} \sim \theta_{zz}V''(\theta_z)$, or $\lambda \sim 2\pi\gamma/(P\sqrt{H})$. As previously discussed [21], treating finite-size fronts as a perturbation of zero-width fronts enables one to convert Hotani's data on angles between coexisting helical states into an estimate of front width, with the result $\lambda \simeq 100$ nm. Combining this with our value for H yields $\gamma^2 \simeq 4 \times 10^{-27}\tilde{U}^*$ erg cm^3 $\simeq 10^{-26}$ erg cm^3, using typical flow rates.

Associated with the various length scales ℓ above are time scales $T(\ell)$. Bends relax on the scale $T_A(\ell) = \zeta_\perp \ell^4/A$, and twist changes on two time scales, depending on whether axial rotation balances the twist-gradient term ($\zeta_r\theta_t \sim \gamma^2\theta_{zzzz}$), giving $T_\gamma \sim \ell^4\zeta_r/\gamma^2$, or the twist potential [$\zeta_r\theta_t \sim \theta_{zz}V''(\theta_z)$], so $T_V \sim (2\pi\ell)^2\zeta_r/(HP^2)$. Relaxation thus occur on two scales: the inner scale λ of the front, with times $T_A(\lambda) \sim 10^{-6}$ s and $T_\gamma(\lambda) = T_V(\lambda) \sim 10^{-8}$ s; and the pitch scale with $T_A(P) = 10^{-1}$ s, $T_\gamma \sim 10^{-3}$ s, and $T_V \sim 10^{-6}$ s. When the system is driven away from equilibrium by a flow (initially introducing a pure *bending* deformation), the initial response will be through a *twisting* deformation. Subsequently, the slow bending relaxation is towards the new twisted state $e^{i\theta}$.

As discussed in detail elsewhere [23], this problem is ripe for treatment with matched asymptotics, with an inner region on the scale of the twist front and an outer region on the scale of the helix pitch (or filament length). Here we scale on the bend time, filament length, and bending modulus, setting $\xi = L\chi$, $z = L\alpha$, $t = (\zeta_\perp L^4/A)\tau$, and $V(\Omega) = Hf(\Omega)$, to obtain

$$\chi_\tau + u\chi_\alpha = -(\chi_{\alpha\alpha} - qe^{i\theta})_{\alpha\alpha}, \qquad (8)$$

$$\epsilon^2\theta_\tau = -w\theta_{\alpha\alpha\alpha\alpha} + hf''(\theta_\alpha/L)\theta_{\alpha\alpha} + q\mathrm{Im}(e^{i\theta}\chi^*_{\alpha\alpha}), \qquad (9)$$

with the dimensionless flow velocity $u = \zeta_\perp L^3 U/A$, spontaneous curvature $q = QL$, drag coefficient ratio $\epsilon^2 = \zeta_r/\zeta_\perp L^2$, potential amplitude $h = L^2H/A$, and twist-gradient stiffness $w = \gamma^2/AL^2$. The bending stiffness of bacterial flagella is not particularly well determined, but estimating from that of the flexible hook gives $A \sim 10^{-14}$–10^{-13} erg cm. Using this range, the dimensionless parameters in (8) and (9) have the typical values $u \sim$ 1–10 for flow velocities of μm/s, $q \sim 10$, $\epsilon^2 \sim 10^{-7}$, $h \sim 10$, and $w \sim 10^{-5}$. This shows that the fluid velocity necessary to make an order-1 change in the shape of the filament is indeed that seen in experiment.

We numerically integrated (8) and (9) for the parameter values given above. The main features observed in Hotani's remarkable experiment are accurately captured; initiation of a chirality reversal at the upstream end of a pinned flagellum, growth and detachment of a pulse from that end, and resetting of the chirality through torque cancellation. The front propagation velocity was shown already in Fig. 2, validating the scaling result (5), with a minimum flow speed for the onset of polymorphism found to be 10 μm/s, close to the measurement of Hotani (a few μm/s). Below this, the helix unwinds slightly from the preferred state and then ceases to move. At and above the critical velocity, we observe (Fig. 3) nucleation, propaga-

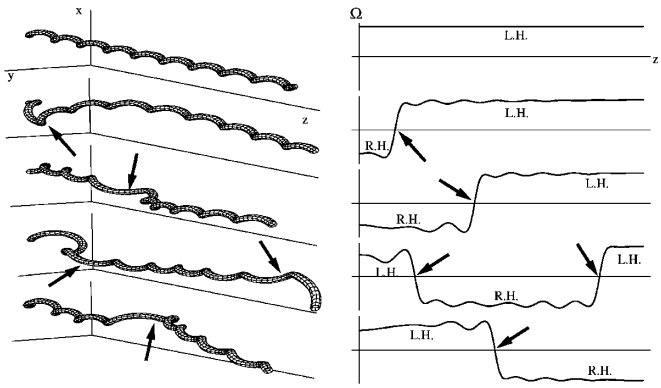

FIG. 3. Filament configuration time series for flow speed close to critical ($U = 10$ μm/s) with corresponding twist-rate (Ω) plots. Time runs from top ($t = 0$ s) to bottom ($t = 11.7$ s). Arrows indicate points at which the handedness changes. The oscillations seen in the twist, while reminiscent of computational artifacts (Gibbs phenomena), are real; they arise from a phase mismatch between the actual and locally preferred pitch of the filament.

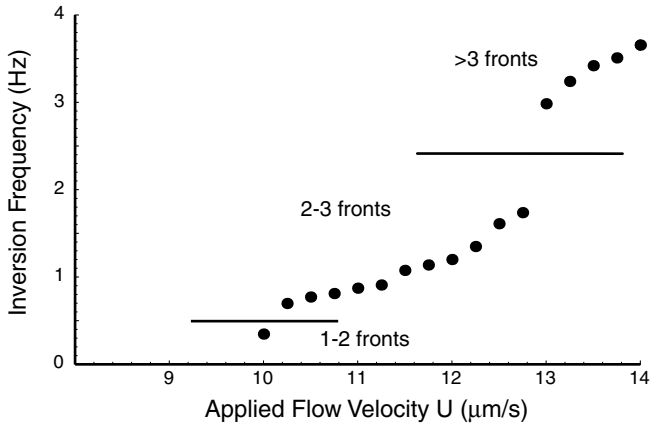

FIG. 4. Numerical results for inversion frequency and number of domains vs fluid speed. Dots are numerically determined inversion frequencies; lines separate regimes in which different numbers of fronts exist simultaneously on the filament.

tion, and resetting of domains. The speed at which a front traverses the filament grows with the applied fluid velocity. The frequency of front nucleation and the number of fronts on the filament at one time increases nontrivially with the flow speed (Fig. 4).

A detailed test of the predictions of this model requires new experiments. We urge that Hotani's experiments be reproduced with, for instance, fluorescently labeled flagella [6] and an optically trapped bead as an anchor point. Using magnetic beads [24], the flagellum may be rotated, permitting full examination of flagellar responses to fluid drags and applied torques. It would also be possible to observe the interaction between multiple flagella under imposed flows and torques, giving insight into the bundling–unbundling transition in swimming cells, although under extensional rather than compressive circumstances. The insight gained here as to how a steady Stokes flow generates oscillating helical chirality may also find applications in micro-fluid-dynamical devices.

We thank Howard Berg, Alain Goriely, Thomas Powers, Wim van Saarloos, and Charles Wolgemuth for important discussions, and Hirokazu Hotani for ongoing correspondence and Fig. 1. This work was supported by NSF Grant No. 9812526 (R. E. G., J. O. K., and G. H.) and the Robert S. Flinn Foundation (D. C.).

[1] H. C. Berg and R. A. Anderson, Nature (London) **245**, 380 (1973).
[2] R. M. Macnab and M. K. Ornston, J. Mol. Biol. **112**, 1 (1977).
[3] K. Namba and F. Vonderviszt, Quart. Rev. Biophys. **30**, 1 (1997).
[4] H. Berg, *Random Walks in Biology* (Princeton University Press, Princeton, 1983).
[5] H. Hotani, J. Mol. Biol. **156**, 791 (1982).
[6] L. Turner, W. Ryu, and H. Berg, J. Bacteriol. **182**, 2793 (2000).
[7] C. R. Calladine, Nature (London) **255**, 121 (1975).
[8] R. Macnab, *Escherichia coli and Salmonella: Cellular and Molecular Biology* (American Society for Microbiology, Washington, DC, 1996), 2nd ed.
[9] F. Samatey *et al.*, Nature (London) **410**, 331 (2001).
[10] R. Macnab, Nature (London) **410**, 321 (2001).
[11] I. Yamashita *et al.*, Nature Struct. Biol. **5**, 125 (1998).
[12] D. L. C. Caspar, Nature Struct. Biol. **5**, 92 (1998).
[13] E. Purcell, Proc. Natl. Acad. Sci. (U.S.A.) **94**, 11 307 (1997).
[14] E. M. Purcell, Am. J. Phys. **45**, 3 (1977).
[15] R. Goldstein, T. Powers, and C. Wiggins, Phys. Rev. Lett. **82**, 1590 (1998).
[16] S. Camalet, F. Jülicher, and J. Prost, Phys. Rev. Lett. **82**, 1590 (1999).
[17] C. Wolgemuth, T. Powers, and R. Goldstein, Phys. Rev. Lett. **84**, 1623 (2000).
[18] M. E. J. Holwill and R. E. Burge, Arch. Biochem. Biophys. **101**, 249 (1963).
[19] J. B. Keller and S. I. Rubinow, J. Fluid Mech. **75**, 705 (1976).
[20] L. Landau and E. Lifshitz, *Theory of Elasticity* (Pergamon Press, Oxford, 1986).
[21] R. Goldstein, A. Goriely, G. Huber, and C. Wolgemuth, Phys. Rev. Lett. **84**, 1631 (2000).
[22] C. H. Wiggins, D. Riveline, A. Ott, and R. E. Goldstein, Biophys. J. **74**, 1043 (1998).
[23] D. Coombs, Ph.D. thesis, University of Arizona, 2001.
[24] T. R. Strick, J.-F. Allemand, D. Bensimon, A. Bensimon, and V. Croquette, Science **271**, 1835 (1996).